Petroleum Science 21 (2024) 3790–3803

Contents lists available at ScienceDirect

Petroleum Science

journal homepage: www.keaipublishing.com/en/journals/petroleum-science

Original Paper

Architectural characterization of carbonate tidal channels in the Mishrif formation, Southeastern Iraq

Zhan-Feng Qiao [a, b, c], Guang-Ya Zhu [d], Shun-Li Li [e, *], Guan-Ming Shao [a], Wen-Jun Kang [e], Xiao-Wei Sun [a], Qian-Ying Yao [a], Yu Zhang [a]

[a] PetroChina Hangzhou Research Institute of Geology, Hangzhou, 310023, Zhejiang, China
[b] CNPC Key Laboratory of Carbonate Reservoir, Hangzhou, 310023, Zhejiang, China
[c] State Energy Key Laboratory of Carbonate Oil and Gas, Hangzhou, 310023, Zhejiang, China
[d] PetroChina Research Institute of Petroleum Exploration and Development, Beijing, 100083, China
[e] School of Energy Resources, China University of Geosciences, Beijing, 100083, China

ARTICLE INFO

Article history:
Received 20 November 2023
Received in revised form
10 May 2024
Accepted 11 July 2024
Available online 18 July 2024

Edited by Jie Hao and Meng-Jiao Zhou

Keywords:
Carbonate tidal channels
Architecture bounding surfaces
Architectural elements
Mishrif formation

ABSTRACT

For a better understanding of the strong heterogeneities of the Mishrif Formation in the H Oilfield of southeast Iraq, the characterization of the carbonate architectures has become one of the key research departments of carbonate rocks. This study aims to reveal the architecture and controlling factors of the carbonate tidal channels in the MB1-2B sub-layer of the Mishrif Formation in response to the delineation of the tidal channels that have hydrocarbon potential. Three architectural elements and three architectural boundaries of the tidal channels were identified by interpreting the cores, well-logging, seismic, and analytical data. The results show that: (1) the architecture characteristics of tidal channels are mainly migrating type in the downstream zone, the side of concave bank of the tidal channels is usually filled with relatively coarse-grained grainstone; (2) the architecture characteristics of tidal channels are mainly swinging type in the upstream zone, showing the high porosity and permeability; (3) the architecture characteristics of tidal channels are mainly vertical-accretion type in the mid-regions, indicating the instantaneous current reversals and high geographical position. This analysis demonstrates that the best reservoir quality within the tidal channels is located in the bend of the tidal channel near the inner lagoon and open sea, it provides the geological models for later exploration and development in the Mishrif Formation.

1. Introduction

The carbonate reservoirs have been considered a very important oil and gas producing formation, accounting for about 47% of the world's total oil and gas reserves (Roehl and Choquette, 1985; Shen et al., 2019). For about half a century, there has been an increase in the classical achievement of carbonate facies during phases of the study of carbonate reservoirs (Wilson, 1975; Read, 1982; Yang and Wu, 1998; Flügel, 2004; Li et al., 2010; Xu et al., 2012; Purkis, 2019), such as Wilson (1975) summarized 24 standard facies types and a carbonate sedimentary model consisting of 3 facies belts and 9 subfacies based on the analysis and discussion of the tide, wave, oxidation interface, salinity, water depth, water circulation, and other factors in the sedimentary environments; Flügel (2004) divided the carbonate rocks into 26 standard facies types and 10 facies belts based on the Wilson's carbonate rimmed platform model; and another practical standard facies type is the carbonate gentle slope model (Read, 1982). Recently, because of the diverse reservoir space, strong heterogeneity, complex origin, and great difficulty in reservoir characterization and prediction (Kerans, 1988; Moore, 2001; Zhao et al., 2012; Léonide et al., 2014; Bosence et al., 2015; Qiao et al., 2016, 2017), the tidal channels in the carbonate facies have become the focus of attention in the petroleum industry (Hashemi et al., 2014; Alqubalee et al., 2022; Noureldin et al., 2023).

The tidal channel is an erosive/constructive channel formed by tidal processes or currents (Grélaud et al., 2010), and controlled by tidal regimes on short timescales and sea level and climate changes

* Corresponding author.
E-mail address: lishunli@cugb.edu.cn (S.-L. Li).

https://doi.org/10.1016/j.petsci.2024.07.013

over long timescales (Ferreira et al., 2022). Understanding the high variability of tidal channel shapes and patterns of sinuosity (Donnici et al., 2017; Ferreira et al., 2022) has been the object of recent studies. The primary controlling factor in tidal channel variability is the increased accommodation during the initial stages of transgressions (Bayet-Goll et al., 2018), the retrogradation of the channel island-ward margin (Wu et al., 2021), the varying hydraulic pressure gradient between the shelf-lagoon and the adjacent ocean basin (Harris et al., 2005), and the velocity of tidal currents (Reeder and Rankey, 2009). There are many documented examples of channel deposits in outcrops (e.g., Rahmani et al., 1988; Rebata et al., 2006; Grélaud et al., 2006, 2010) and modern studies (e.g., Hubbard et al., 2011; Davis and Dalrymple, 2012; Hein et al., 2013; Olariu et al., 2015). For example, the coarse sheets represent high energy tidal channels (Tirsgaard, 1993); tidal channels in the toward upstream networks are mainly infilled by fine-grained sediments due to decreasing energy (Hughes, 2012; Ferreira et al., 2022); the base of the tidal channel in the shallow-water tidal setting could be infilled by the massive grainstones (Reynaud and James, 2012); the scour-based fining-up dolostone beds are interpreted as shallow channel/tidal channel fills (Seyedmehdi et al., 2016; Pratt and Rule, 2021); the meter-scale channel form is filled with bio-grainstone in the middle and upper parts of the succession (Salehi et al., 2020); and the channel within the channelized zone possibly have mud-covered bottoms, but locally shelly lags occur (Wu et al., 2021).

In recent years, the study of architectural elements is relatively mature in the research of clastic reservoirs (Williams and Rust, 1969; Miall, 1977, 1985, 1988, 1992, 1993, 1996, 2014, 2022; Cant and Walker, 1978; Bluck, 1979; Allen, 1983; Walker and Cant, 1984; Bridge, 1993, 2003; Lunt and Bridge, 2004; Bridge and Lunt, 2006; Li et al., 2015), which laid the foundation for later study of the architecture of carbonate bodies (Jin, 2009; Chen et al., 2015; Chang et al., 2018; Kargarpour, 2020; Zhu et al., 2021). Since the architecture of tidal channel proposed by Tirsgaard (1993), numerous models were established including the isolated and downdip geometry for channel complex filled with carbonate grainstone (Rankey, 2003), the lenticular bodies (ooidal grainstone and ooid-intraclast packstone/grainstone) with erosional bases (Armella et al., 2007), the laterally accreted tidal bars and forward-accreted tidal dunes in large tidal channels (Chen et al., 2022), the “circular” fill of the tidal channel (Olariu et al., 2015), and the lateral/vertical accretion geometries of the tidal channels during flooding of the carbonate platform (Grélaud et al., 2006, 2010). Despite studies of internal filling and external shape, the architecture classification and hierarchy of the tidal channel are still poorly understood because of the complicated interaction between erosional and depositional processes.

In addition, tidal channels are characterized by strong heterogeneity due to their mode of deposition (Noureldin et al., 2023) and the bioturbation that has a negative impact on the reservoir quality of tidal channels (Alqubalee et al., 2022). According to the discrepancy between the reservoir properties and surrounding rock, Noureldin et al. (2023) performed post-stack inversion techniques to delineate the hydrocarbon-bearing tidal channel contained in the carbonate reservoir; Sabouhi et al. (2023) distinguished the position and geometry of channels by acoustic impedance; Hashemi et al. (2014) utilized Multiple-point statistics to simulate a channelized carbonate reservoir located southwest Iran; and Ferreira et al. (2022) summarized the patterns of internal reflections, terminations, and outer shapes for tidal channel base on high amplitude, low frequency, and low lateral continuity. Moreover, delineating tidal channels in the carbonate reservoir is crucial to diminish drilling risks, and raise the hydrocarbon potential (Noureldin et al., 2023). Hence, the architectural characterization is significantly needed for the reservoirs of the tidal channel.

In the study area, the research on the reservoir architecture of Mishrif Formation in H Oilfield is mainly based on cores, cast thin-sections, well-logging, seismic and other data, and the reservoir architecture of lagoon facies, bioclastic shoal facies, tidal channels, and other facies were analyzed within the framework of fourth-order sequence (Sun et al., 2020). Despite reservoir architectures being constructed in the injection-production well groups, the research mainly focuses on the description of the architecture boundary of facies and the establishment of the reservoir architecture model in the fourth-order sequence. However, there was a lack of in-depth analysis of the internal texture and reservoir predictions of typical architectures such as carbonate tidal channels on a smaller scale. This paper aims to classify the carbonate tidal channel architecture, identify the multiple-order boundaries of the tidal channels based on cores, well-logging, and seismic data, finely depict the external shape and internal structure of tidal channel architectures, characterize its spatial distribution and superposition patterns, and establish a geological model reflecting the genesis of sedimentation, which will provide the geological basis for the fine development of carbonate reservoirs in H Oilfield.

2. Geological settings

The H Oilfield is located in Misan Province in the southeast of Iraq in the northeast of the Arabian Plate (Aqrawi et al., 2010; Al-Qayim, 2010) (Fig. 1), tectonically located in the foredeep zone of Mesopotamia Basin, is an NW-SE trending broad and gentle long axis anticline formed in the Neogene Zagros orogeny (Dunnington, 2005). The H Oilfield, located on the border of Iran and Iraq and the Basra area, is distributed in a strip in the southeast direction (Fig. 1).

The Mishrif reservoir has been found in most fields from central Iraq as far north as the Hamlin Mountains and throughout southeastern Iraq (Dunnington, 2005). The Mishrif Formation was developed in the Tigris River Basin through East Baghdad and Halim in the northeast. The average thickness of the formation in Amara, H Oilfield, and other areas is 350–400 m, while it becomes thinner and pinches out in the west and southwest (Aqrawi, 1998). The thickness of the formation in Well Zubair-3 is only 157 m. The Late Albian-Early Turonian stratigraphic structure represents a transition from the onlap margin to the basin, with the late Rumaila Formation moving upwards into the Mishrif Formation near the east and north, and northeastward into the Iraqi Kurdistan region near the southeastern Kirkuk Oilfield. Therefore, the Mishrif Formation became the Dokan and Balambp Formation (Aqrawi et al., 2010). The Mishrif Formation, first described by Owen and Nasr (1958) from southern Iraq, overlies the Rumaila Formation carbonates in the zone between the Iraq-Iran border and the Basra region in southwestern Iraq, and is characterized by strong heterogeneity (Sadooni, 2005; Wang et al., 2016).

The Cretaceous Mishrif Formation of the H Oilfield in Iraq was divided into 4 members (MA, MB1, MB2, and MC) and 15 submembers, constituting 5 third-order sequences (Sun et al., 2020). The top surface of each third-order sequence was bounded by typical facies types such as tidal channels, incised valleys, or unconformity surfaces representing sea-level fall (Sun et al., 2020). The main production layers of the oilfield are MB2 and MB1, where a large number of relatively low-energy fine-grained carbonate rocks (mainly argillaceous or marlite) were developed, accounting for 59.74% of the reserves, with significant oil and gas development potential (Sun et al., 2020). The MB2 Member of the Mishrif Formation was a high-energy, coarse-grained bioclastic grain limestone reservoir with a thickness of about 30 m, good physical properties, and high production. The MB2 Member was developed with a thick-bedded bioclastic shoal, which was mainly affected by

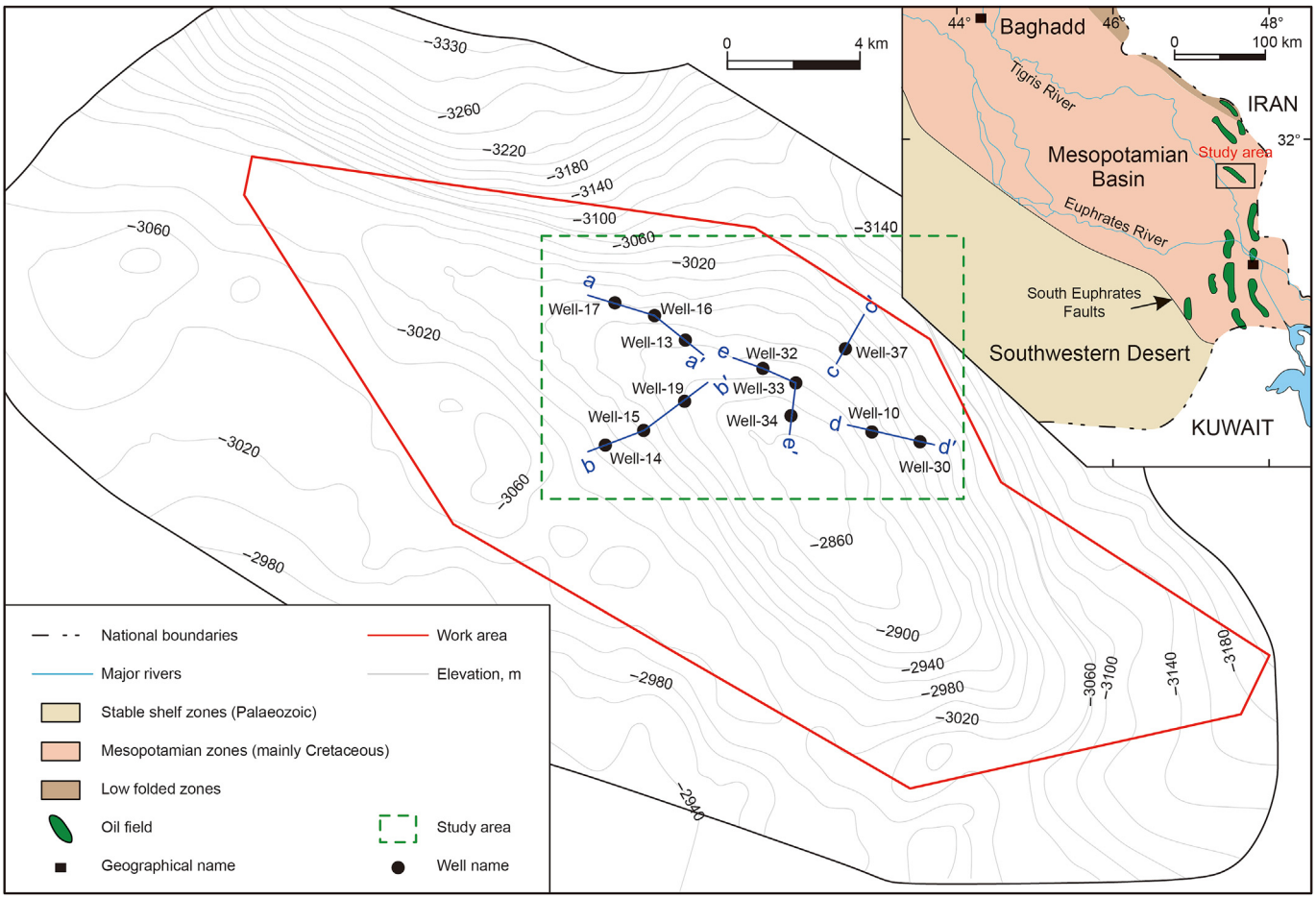

Fig. 1. Location of main structural areas in the study area and structural map of the top surface of MB1-2A. The main tectonic regions were modified from Aqrawi (1998); map of the study area in southern Iraq showing the location of wells investigated, and the range of profiles and planes presented in Figs. 7 and 8.

the dissolution of atmospheric freshwater, with the most significant dissolution and the largest pore throats, and were the best reservoirs in the Mishrif Formation (Yu et al., 2018). The MB1 Member of the Mishrif Formation showed a thickness of 100 m and was divided into MB1-1 and MB1-2 sub-members, of which the MB1-1 sub-member was mainly composed of dense micrite limestone with a thickness of about 10–20 m, and no reservoir was developed. The MB1-2 sub-member was further subdivided into three sub-layers, namely MB1-2A, MB1-2B, and MB1-2C (Fig. 2), which were composed of the fine-grained carbonate rocks dominated by packstone and wackestone, intercalated with the coarse-grained bioclastic limestone, with large reserves and strong reservoir heterogeneity (Sun et al., 2020).

The stratigraphic framework in this paper mainly adopted the vertical and horizontal analysis and comparison of sequence boundaries of representative wells in several oilfields in southern Iraq by Mahdi and Aqrawi (2014). The T-R sequence division method was employed to identify three third-order sedimentary sequences S1, S2, and S3 (Fig. 2), as well as the fourth-order sequence subdivided by Sun et al. (2020). A thin layer division scheme was established (Fig. 2). The S2 and S3 were composed of transgressive and regressive (T-R) cycles, and the regressive stage was dominant. Transgressive cycles were interpreted as transgressive system tracts (TSTs), while regressive cycles were interpreted as highstand system tracts (HSTs); maximum flooding surfaces (MFS) represent transition points between transgression and regression (Fig. 2).

3. Methods

3.1. Datasets

Data used include more than 30 thin sections of core samples in the Mishrif Formation from well-16 distributed across the northern of the H Oilfield (Fig. 1). Some thin sections were stained with Alizarin Red S to differentiate dolomite from calcium carbonate. The analyzed samples were collected at 1 m depth intervals. The definition of their grain types, depositional textures, and diagenetic features was based on a combination of classifications and terminology of Dunham (1962), and Embry and Klovan (1971), respectively.

Petrographic observations led to the definition of facies (described by Mahdi et al., 2013), which were based on the classification schemes of Wilson (1975) and Flügel (2004). The facies interpretation was supported by the log interpretation and core description. In this study, the color, grain size, texture, and sedimentary structure of the core samples were depicted in detail, which were the main components of facies description in the Mishrif Formation. The electric log suites of gamma-ray, sonic, and neutron logs were used to correlate facies in non-cored intervals of the studied wells, as each facies association has some distinctive log signatures that can be easily tracked vertically and laterally between the wells. For instance, the sharp contacts of the gamma-ray curves generally represent the erosive base of the channels, and the spurs of the blocky gamma-ray curves indicate the muddy layers

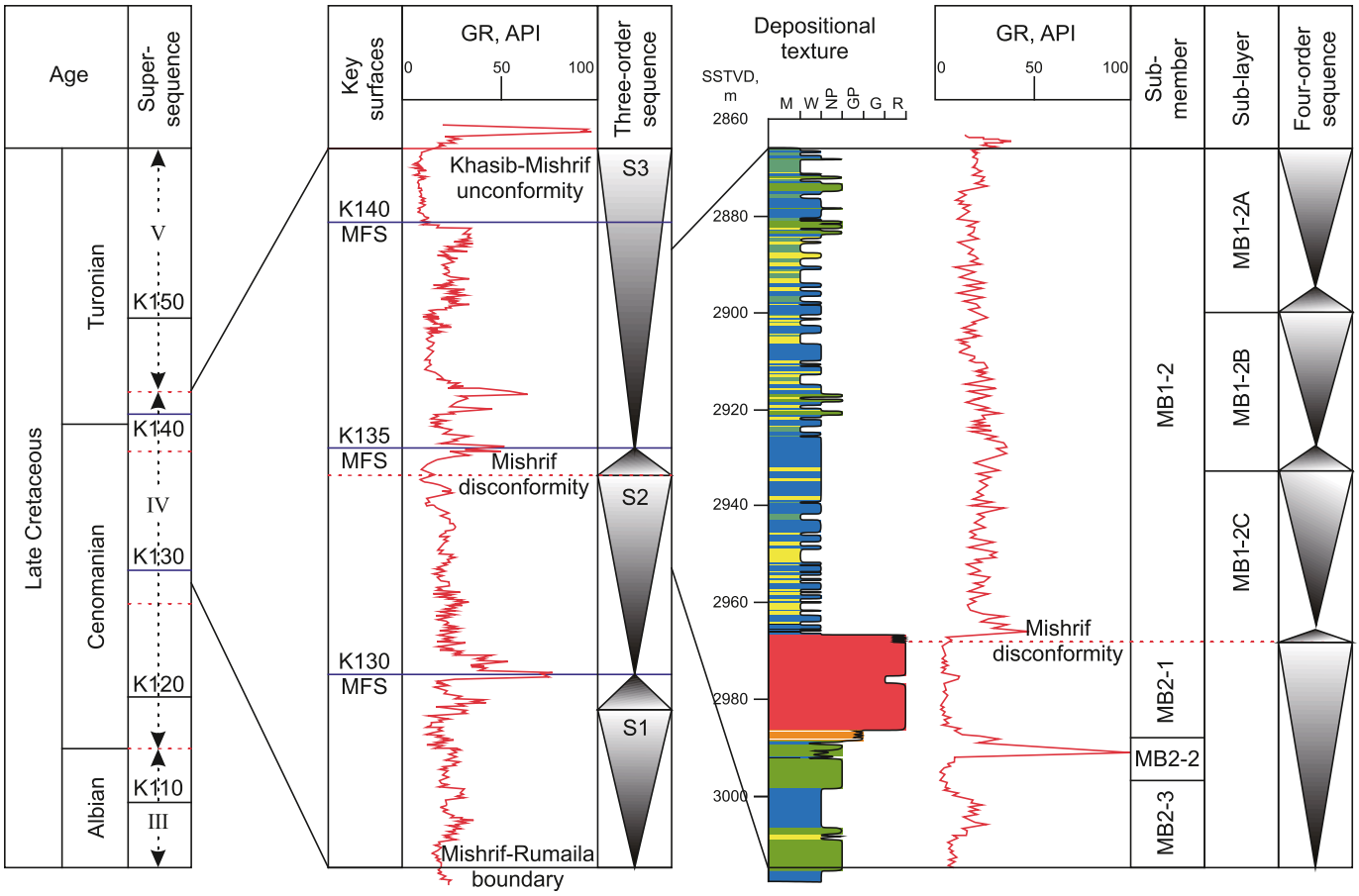

Fig. 2. Stratigraphic and sequence characteristics of the studied intervals. Generalized stratigraphy, major regressive cycles, key surfaces identified, and three-order sequences of the Mishrif Formation modified from Mahdi et al. (2013). Four-order sequences, sub-members, and sub-layers in this study were used for architectural analysis (modified from Sun et al., 2020).

within the grainstones.

Well correlation lines were selected to show the architecture classification of tidal channels (Fig. 1, a–a′). Five well correlation lines and a plane of attribute inversion were selected to show the spatial distribution characteristic of the tidal channels (Fig. 1). Available wireline logs (Gamma-ray, Sonic, and Neutron) were used to predict and correlate architectural surfaces in uncored intervals.

The sparse impulse impedance inversion results were used for both the sections and planes. The method of inversion is mainly used to extract reflection coefficients from the original seismic traces, then let them be folded with wavelet to produce seismic traces, and then modify the number of reflection coefficients by the residual difference between the generated traces and the original traces, and then produce new synthetic seismic recording traces, and so on to stop the iteration to get the final inversion results when the residual difference is minimized.

3.2. Hierarchy of tidal channel architectural boundaries

Although carbonate facies studies are continuing to generate variations due to biochemical action, there are many points of similarity in the channel between carbonate rock architecture and clastic rock architecture.

1) Smaller elements of the channel form stacked complexes within larger elements of the channel (Rankey, 2003), and these elements can form a hierarchy of scales (Allen, 1983), such as the groups of elements or complexes usually are well-defined erosion surfaces (Miall, 1985).
2) Channel-fill complexes contain several types of elements (Miall, 1985), including the channel element, and the deposits of the other types of elements (eg., lateral accretion deposits, overbank fines; Chen et al., 2022) within the channel-fill complexes.
3) Provide channel models (Miall, 1985) to illustrate the geomorphology and channel architectures of tidal channel systems (Tirsgaard, 1993).

Therefore, referring to the clastic rock architecture classification (Miall, 1977, 1985, 1996), the channelized carbonate rock architecture was classified as follows (Fig. 3). The 0-order boundary: sedimentary lamina (sediment structure) surface; the 1st boundary: the surface of cross-bedding sets; the 2nd boundary: the surface between lithofacies (geological facies); the 3rd boundary: the surface between lithofacies association (sedimentary sequence or channelization); the 4th boundary: the surface between facies (single tidal channel); the 5th boundary: facies combination bounding surface (tidal channel complex); the 6th boundary: subfacies bounding surface (tidal channel-delta system); the 7th boundary: facies belt bounding surface (equivalent to the 4th-order stratigraphic sequence). In this study, the 4th and 5th boundaries were the main objectives to describe. For non-channelized carbonate rock architecture, such as the shoal, the 0-order to 3rd boundary is similar to the channelized carbonate rock architecture. The 4th boundary: the surface between facies (single shoal); the

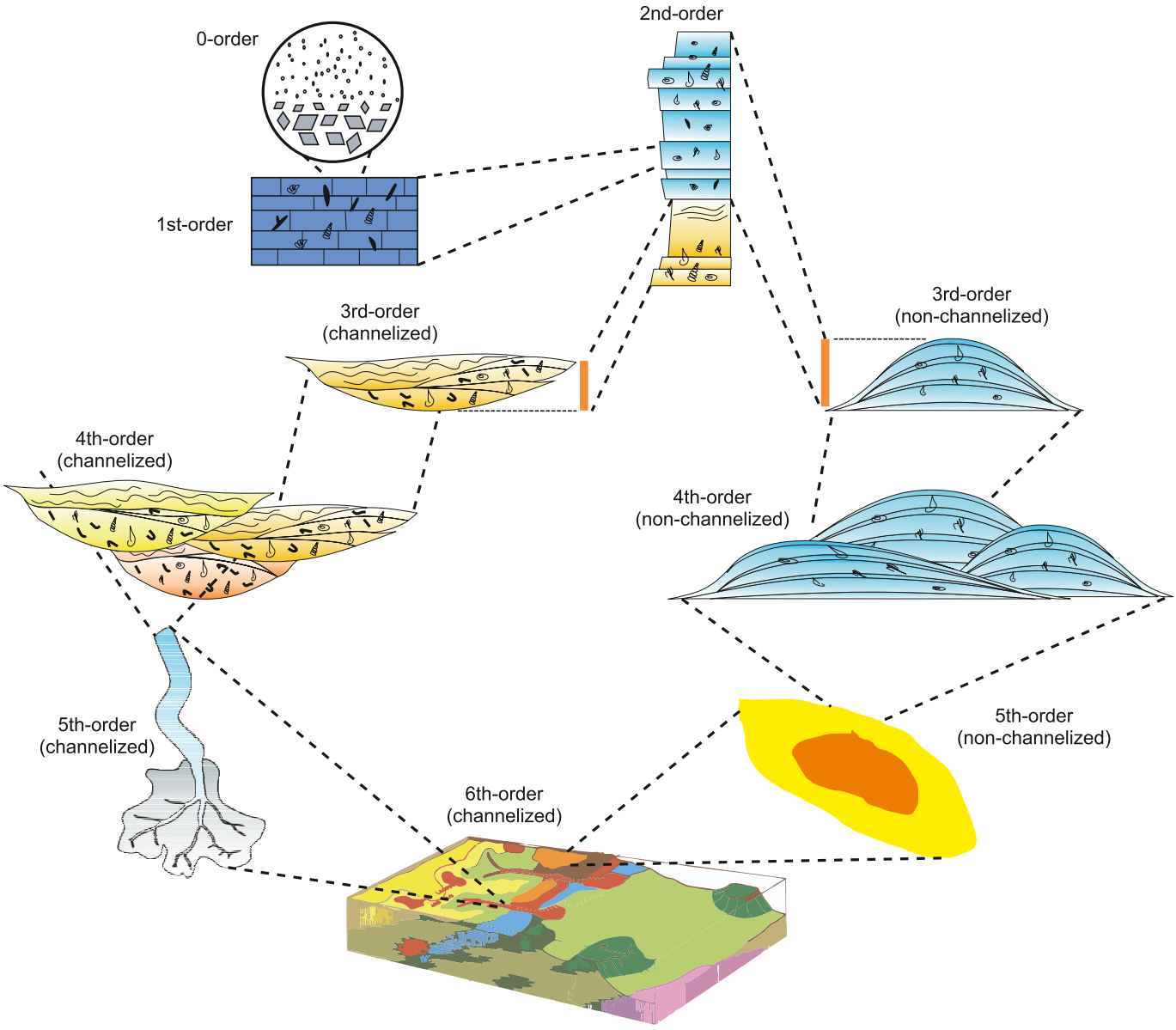

Fig. 3. Carbonate rock architecture and bounding surface classification.

5th boundary: facies combination bounding surface (shoal complex); the 6th boundary: subfacies bounding surface (shoal-lagoon system).

4. Characterization of tidal channel architectures in the Mishrif formation

4.1. Architectural boundaries of tidal channels

The identification and division of the architectural boundaries were carried out by lithofacies assemblages, impedance inversion, and the variation of the logging curves. Five types of boundaries were identified (Figs. 4 and 5): the top and bottom surfaces of the tidal channel complex were 5th-order architecture boundaries; the top and bottom bounding surface of a single tidal channel (single facies) were the 4th-order architecture boundaries; the bounding surface between lithofacies combinations (internal channelization) was the 3rd-order architecture boundary; the bounding surface between the same lithofacies was the second-order architecture boundary, and the bounding surface of laminae group was the 1st-order architecture boundary.

4.1.1. Lithofacies and lithofacies assemblages

In the well-16, four lithofacies were identified and combined into four lithofacies assemblages (Fig. 6). The lithofacies of the cross-laminated grainstone consist of unidirectional or rare bidirectional ripple cross-laminated in grainstone. The cores showed a bi-directional arrangement of grayish-white grains with a slight scouring. The bioclasts were well sorted, partly closely packed, and dominated by echinoderms and bivalves. The lithofacies of the cross-laminated grain-dominated packstone consist of grain-dominated packstone with dark brown and light brown interstratified, with inconsistent dip of laminae (Fig. 6). Bioclasts were mainly echinoderms, foraminifera and bivalves, and some peloids. The lithofacies of the structureless mud-dominated packstone were composed of massive mu-dominated packstone with brown-gray.

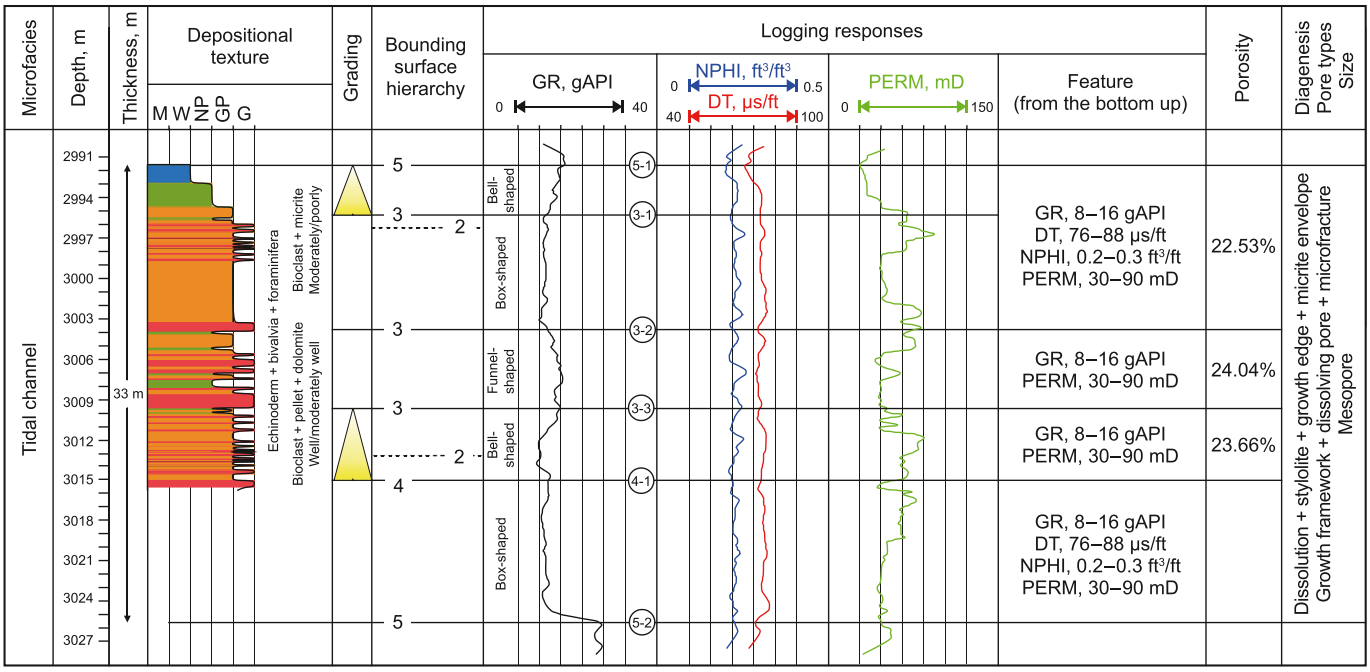

Fig. 4. Tidal channel architecture classification and logging curve response characteristics. The definition of their grain types, depositional textures, and diagenetic features was based on a combination of classifications and terminology of Dunham (1962) and Embry and Klovan (1971), respectively.

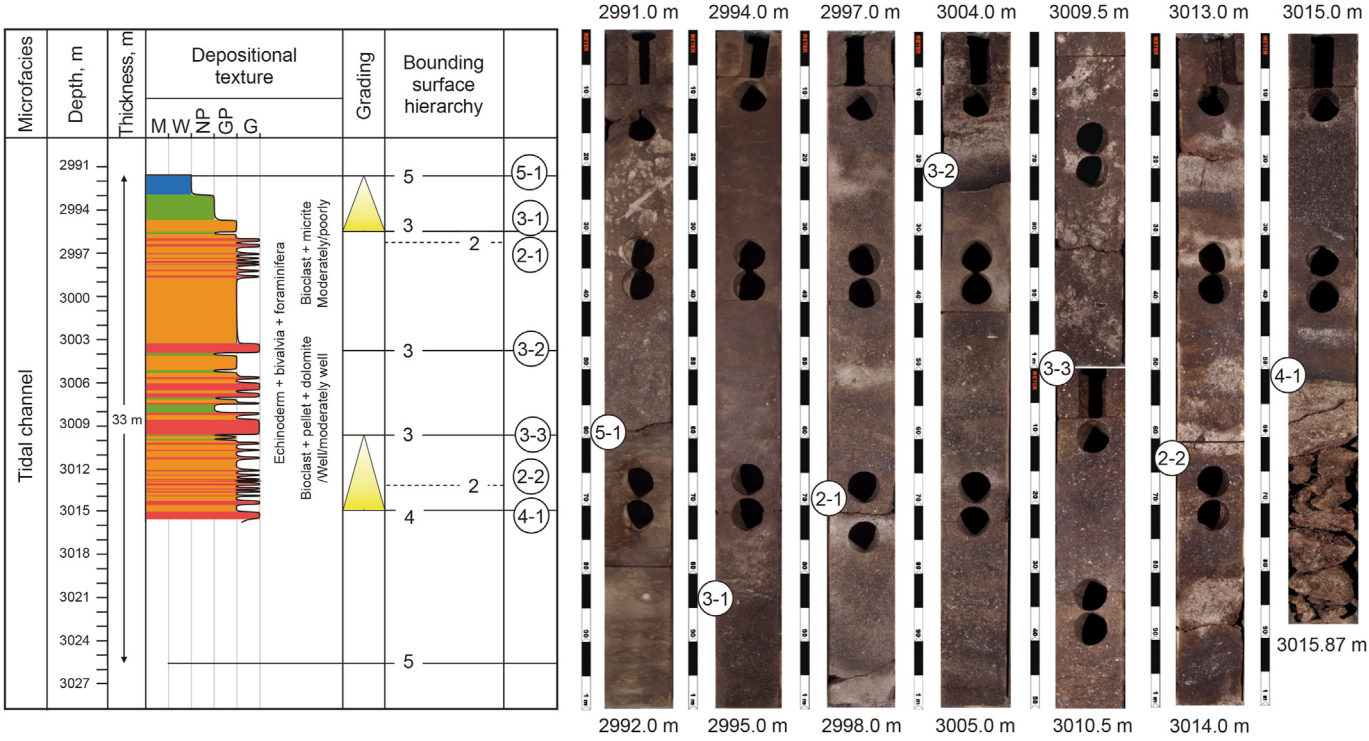

Fig. 5. Rock characteristics of the bounding surfaces of tidal channel architecture.

The content of the bioclastic was moderate, which was dominated by echinoderms and bivalves, and a few foraminiferas. The lithofacies of the mud drapes wackestone consist of thickly bedded wackestone with muddy strips, showing porphyritic features on the cores. The content of the bioclastic was low and dominated by echinoderms and bivalves. Large numbers of micrites and dolomite can be identified in thin sections (Fig. 6).

The overall grain sorting was medium-good sorting, and the biodetritus type was mainly echinoderms, foraminiferas, and bivalves. The structural components were mainly biodetritus and mortar (micrite), and some intervals contained spheroid and a small amount of dolomite. The pore type was mainly secondary pores, including intergranular dissolution pores, intragranular dissolution pores, moldic pores, and a small number of fractures

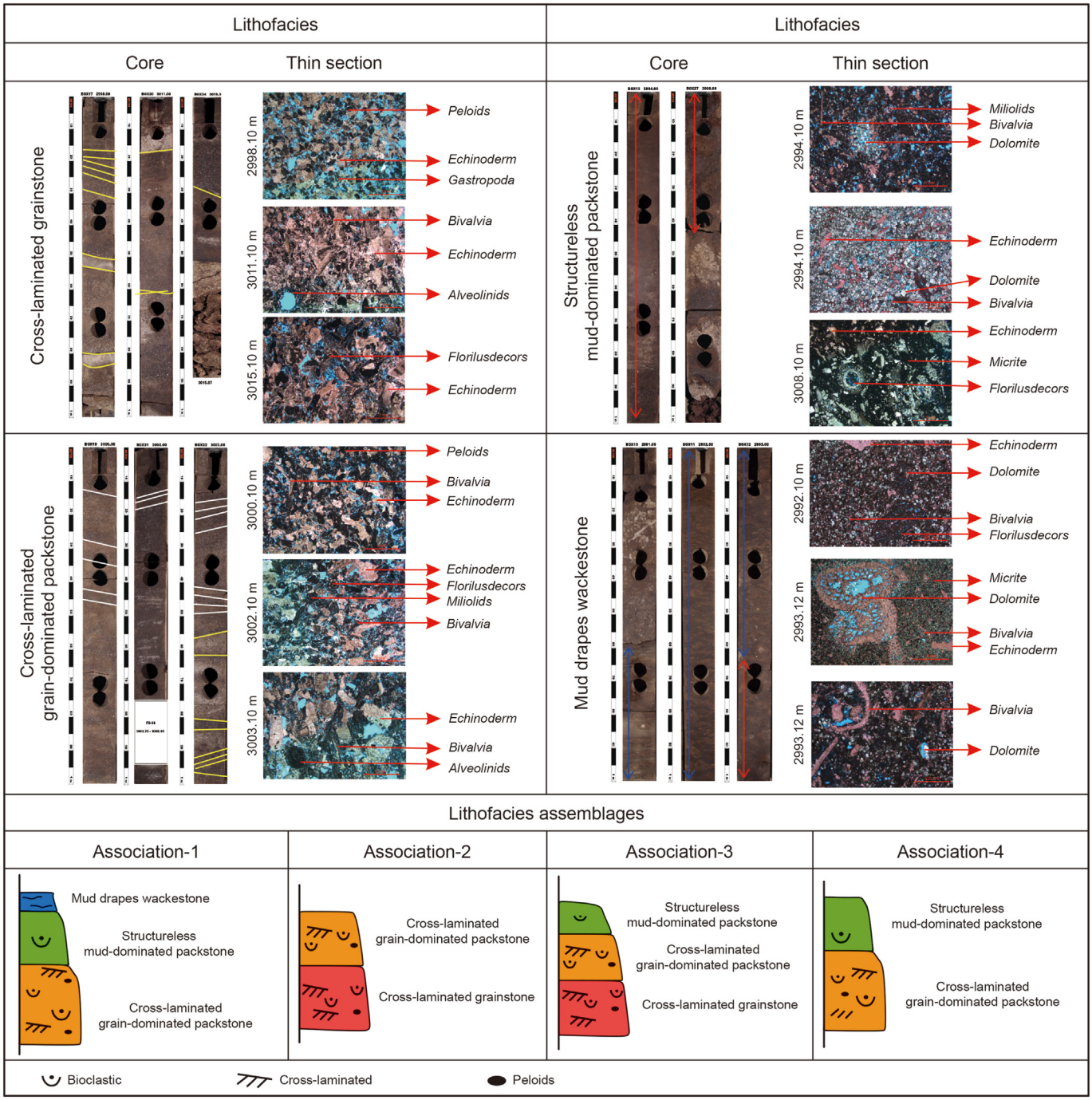

Fig. 6. Generalized summary of lithofacies and lithofacies assemblages identified in the deposits of the tidal channel of the MB1-2B sub-layer, Mishrif Formation, H Oilfield, Iraq.

and intercrystalline dissolution pores. The pore size was mainly mesopore, and some intervals were mainly micropores; the diagenesis was mainly dissolution and cementation, and a small amount of dolomitization, stylolite structure (filled with dolomite) and coaxial growth edge was developed in some intervals.

In the unit of tidal channel, four lithofacies assemblages were identified: association 1 (A1), association 2 (A2), association 3 (A3) and association 4 (A4) (Fig. 6). Association 1 consists of cross-laminated grain-dominated packstone, structureless mud-dominated packstone, and mud drape wackestone from bottom to top. Association 2 includes the cross-laminated grainstone and cross-laminated grain-dominated packstone from bottom to top. Association 3 contains the cross-laminated grainstone, cross-laminated grain-dominated packstone, and structureless mud-dominated packstone from bottom to top. Association 4 consists of the cross-laminated grain-dominated packstone and structureless mud-dominated packstone from bottom to top.

4.1.2. Architectural boundaries

4.1.2.1. The third-order architectural boundary. The bounding surfaces between the lithofacies associations were 3rd-order architecture boundaries, whose lithological identification marks were gradational bounding surfaces (no erosion) between the association 4 and association 2 (Figs. 5, 3-3 and 3-2), and the gradational

bounding surfaces (no erosion) between the association 3 and association 1 (Figs. 5, 3-1), The logging curve GR response characteristics of this architecture bounding surfaces were successively the bounding surfaces between the lower blocky and the upper bell-like shape (Figs. 4, 3-1), the bounding surface between the lower bell and the upper funnel (Figs. 4, 3-3), and the bounding surface of the lower funnel to the upper blocky (Figs. 4, 3-2). There were three types (four channelized bodies) of sedimentary bodies (within the upper channel type) formed by the third and fourth or fifth-order structural bounding surfaces: (1) association 1 (Figs. 5, 3-1 to 5-1); (2) association 2 (Figs. 5, 3-2 to 3-1, 4-1 to 3-3); and (3) association 2, association 3 and association 4 (Figs. 5, 3-3 to 3-2).

4.1.2.2. Fourth-order architectural boundary. The top and bottom surfaces of the single tidal channel (single facies) were 4th-order architecture boundaries, and the lithological identification mark was the local erosion of the channel bottom (Figs. 5, 4-1), which reflected the beginning of channel sedimentation. The logging curve response characteristics of the architecture boundaries are listed as follows: the end of the blocky low-value area (8–10 g API) in the blocky-shaped GR curve of the 4th-order architecture unit was shown as a small mutation surface on the blocky curve (Fig. 4 and 4-1). The lithofacies evolution of the sedimentary body composed of the 4th- and 5th-order architecture boundaries were divided into two stages: the first stage was presumed to be an association 2, the blocky-shaped GR logging response with a similar logging response of channelized bodies in the interval of 3003–2996 m (Figs. 4, 5-2 to 4-1). The second stage consists of association 2–association 3–association 2–association 4–association 2–association 3–association 1 from bottom to top. The GR logging response characteristics were bell-shaped–funnel-shaped–box-shaped–bell-shaped (Fig. 4 and 4-1 to 5-1).

4.1.2.3. Fifth-order architectural boundary. The top and bottom bounding surfaces of the tidal channel complex were the 5th-order architecture boundary, and one of the lithological identification marks was that the top of the complex was often covered by mud drapes. It marked the bounding surface between different sedimentary architectures (the beach body in the study area). The log characteristics of the complex were (Fig. 4): GR showed superposition between blocky and bell-like patterns (8–16 gAPI); DT was weakly blocky-shaped (46–88 us/ft); NPHI was weakly blocky-shaped (0.2–0.3 ft^3/ft^3); PERM was jagged (30–100 mD). The lithofacies evolution of the sedimentary body from bottom to top was listed as follows: association 2 (this interval is not cored, which is speculative; Fig. 7)–association 3–association 2–association 3–association 2–association 4–association 2–association 3 –association 1.

4.2. Architectural elements

Tidal channel elements commonly consist of grainstone, packstone, and wackestone, with a basal concave-up erosional surface. The tidal channel elements in this paper refer to single channel bodies bounded by 4th-order boundaries, ranging in thickness from 8 m to 24 m and in width from 500 m to 1500 m. Architectural elements were defined based on the geometry, type, and proportion of sedimentary structures, and the constituent lithofacies or lithofacies assemblages of the genetic units. Tidal channel units were identified and arranged into three types: swinging tidal channel element (TCHs), migrating tidal channel element (TCHm), and vertical-accretion tidal channel element (TCHva).

4.2.1. Swinging tidal channels (TCHs)

According to the seismic wave impedance inversion profile, the swinging tidal channel was approximately 1500 m wide with a maximum depth of about 24 m. It showed an asymmetric cross-section with a margin steeper on the left than the margin on the right (Fig. 7). The initiation of the erosion surface starts a few decimetres below the former channel deposits (grainstone). The swinging channels were composed of a high proportion of stacked grainstone to grain-dominated packstone with rudist fragments, bivalves, and echinoids.

These channelized bodies generally show the trough cross bedded stratifications (Fig. 7) indicating a dominant current direction (Grélaud et al., 2010). The occurrence of the mud drapes on the upper to top of this swinging channel (Fig. 7), suggested a tidal influence (Olariu et al., 2015). The top of this swinging channel was overlain by a conglomerate with large fragments of corals and rudists (Fig. 7). Four channelized bodies under 3rd-order architectural surface constraints can be identified in the channel fill. This small interbedding of the grain-dominated packstone-grainstone may record a variation of current velocity in the channel (Tirsgaard, 1993; Reeder and Rankey, 2009). Based on previous similar studies of tidal channels (Grélaud et al., 2010) suggesting this erosive structure corresponds to a rise of relative sea level, the swinging of channels was probably controlled by tidal currents and floods.

4.2.2. Migrating tidal channels (TCHm)

The migrating tidal channels (Fig. 7), without core evidence, were similar to the channelized bodies of swinging tidal channels (Figs. 4, 2997–3015 m) on the logging response characteristics. Therefore, the migrating tidal channels may consist mainly of the grain-dominated packstone. According to the seismic wave impedance inversion profile, this tidal channel was formed by the rightward offlapping lateral stack of lens-shaped channelized bodies (Fig. 7), with a width of 700–800 m and thickness of up to 8–10 m (Fig. 7).

The geometry of the erosion surface and the relations with the underlying deposits of the substratum were comparable to those described previously for the swinging tidal channels. Notably, the overall geometry of the migrating tidal channels was near-symmetrical, which was characterized by the sigmoid body that drapes the erosion surface. This lateral deposit transition occurs along broad low-angle inclined stratifications suggesting a process of lateral accretion on the margins of the channel (Grélaud et al., 2010). The lateral accretion geometry of migrating tidal channels was different from the asymmetrical of common migrating channels due to the lateral migration of superimposed, unidirectional bedforms (Li et al., 2015; Andreucci et al., 2017). As with the previous study (Grélaud et al., 2010), the occurrence of these migrating tidal channels shows the development of strong currents during the maximum flooding period of the inner platform.

4.2.3. Vertical-accretion tidal channels (TCHva)

According to the seismic wave impedance inversion profile and the logging interpretation (Fig. 8, e–e′), the vertical-accretion tidal channel contained mudstone and wackestone deposits more than the two other channel types. According to the characteristics of the logging curves, the vertical-accretion tidal channels in the vertical direction show two phases: (1) the lower tidal channel GR shows the bell-shaped, presumed to be association 3 and association 1; the impedance inversion value of the upper tidal channel is higher than that in the lower tidal channel, and the characteristics of GR in the middle of the tidal channel are similar to the GR curve characteristics of the interval of 3009–3005 m (Fig. 4), presumed to be association 4. On the whole, this type of tidal channel was a vertical-accretion tidal channel, without internal lateral migration characteristics.

The relatively fine-grained deposits with muddy composition in

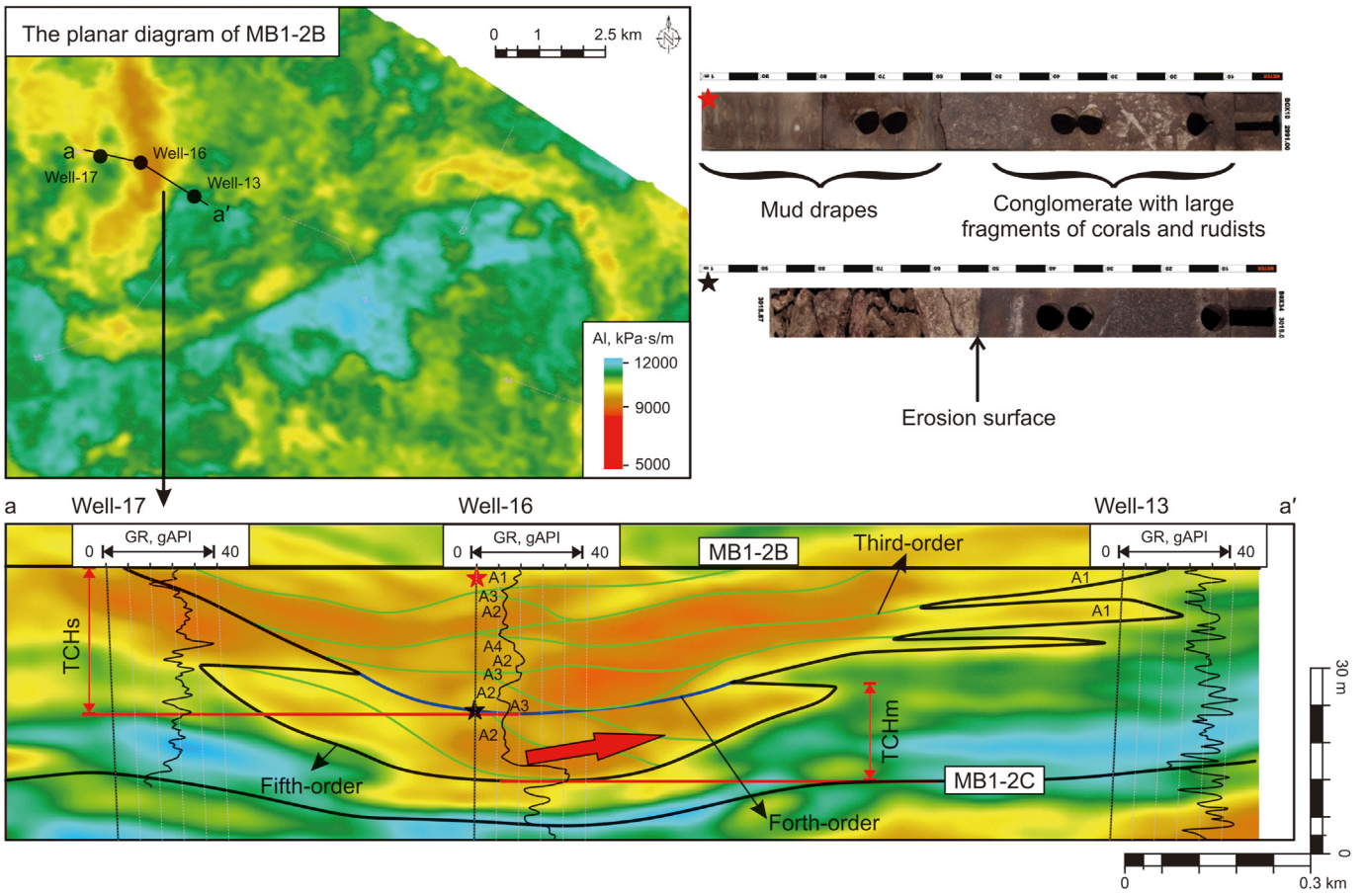

Fig. 7. Internal structure and external shape of the tidal channel architecture. The wave impedance inversion map of MB1-2B shows the locations of cored well-16, non-cored well-17, and well-13. Wave impedance inversion represents the part reservoir. Sinuous planform geometries are present. The seismic profile of a-a′, which passes through well-16, well-17, and well-13, represents an oblique strike section across a sinuous form (tidal channel). The pentagram indicated the sampling location of core photos. Red arrows indicate the migration direction of the tidal channel.

this element indicate low energy of flows (Armella et al., 2007; Li et al., 2015). Therefore, vertical-accretion tidal channels may result in abandoned tidal channels.

5. Sedimentary models of the carbonate tidal channel

5.1. Sectional correlation of tidal channels

It can be seen from the seismic wave impedance inversion profile that the longitudinal profile (generally inclined to the tidal channel) and the transverse profile of the sedimentary body show an asymmetric cross-section of “flat top and concave bottom” (Figs. 7 and 8), and the asymmetry depended on the inclined angle. Bending amplitude characteristics can be observed from the seismic wave impedance inversion plan of the MB1-2B sub-layer (Figs. 7 and 8), which may be channel deposits. Therefore, this kind of sedimentary body is named as tidal channel facies in this study.

From the seismic attribute slice, different sections of tidal channel architecture show different profile structures and spatial superposition characteristics. The tidal channel architecture of the MB1-2 sub-member showed morphological characteristics similar to the meandering channels (Fig. 8). Thus, the tidal channels with a certain degree of curvature present an asymmetric structure. According to the results of seismic attribute inversion, one side of the gentle slope of the asymmetric tidal channel architecture is usually filled with relatively coarse-grained grainstone (Fig. 7, a–a′; Fig. 8, b–b′, c–c′), which is similar to the point bar deposit of a meandering river. While the steep slope side is filled with relatively fine-grained marl (Fig. 7, a–a′; Fig. 8, b–b′, c–c′), similar to the mud plug of a meandering river. When the curvature of the tidal channel architecture is reduced, the interior of the tidal channel is of swinging type (Fig. 7, a–a′; Fig. 8, d–d′), and the sediments are mainly grain-dominated packstone. When the curvature of the tidal channel architecture is straight, the interior of the tidal channel is of filling type (Fig. 8, e–e′), and the sediments are mainly grain mud-dominated packstone and wackestone.

According to the inter-well correlation, the vertical thickness of the carbonate tidal channel architecture complex (level 5) was about 33 m, and the lateral range extended to 1.5 km, of which the thickness of the single-stage tidal channel architecture (level 4) was 4–8 m, and the lateral extension range was about 400–1100 m. According to the description of the boundary and internal structure of the tidal channel architecture (third-order), the tidal channel architecture can be further subdivided into swinging-, migration- and filling-type. Among them, the third-order elements in the swinging tidal channel show the characteristics of bidirectional superimposed migration, generally with large thickness, and the filling lithology is mainly grainstone (Figs. 7 and 8). The third-order elements in the migrating-type tidal channel architecture are characterized by unidirectional migration, medium thickness, and filled with grainstone and marl (Figs. 7 and 8). The third-order element in the filling-type tidal channel architecture is the

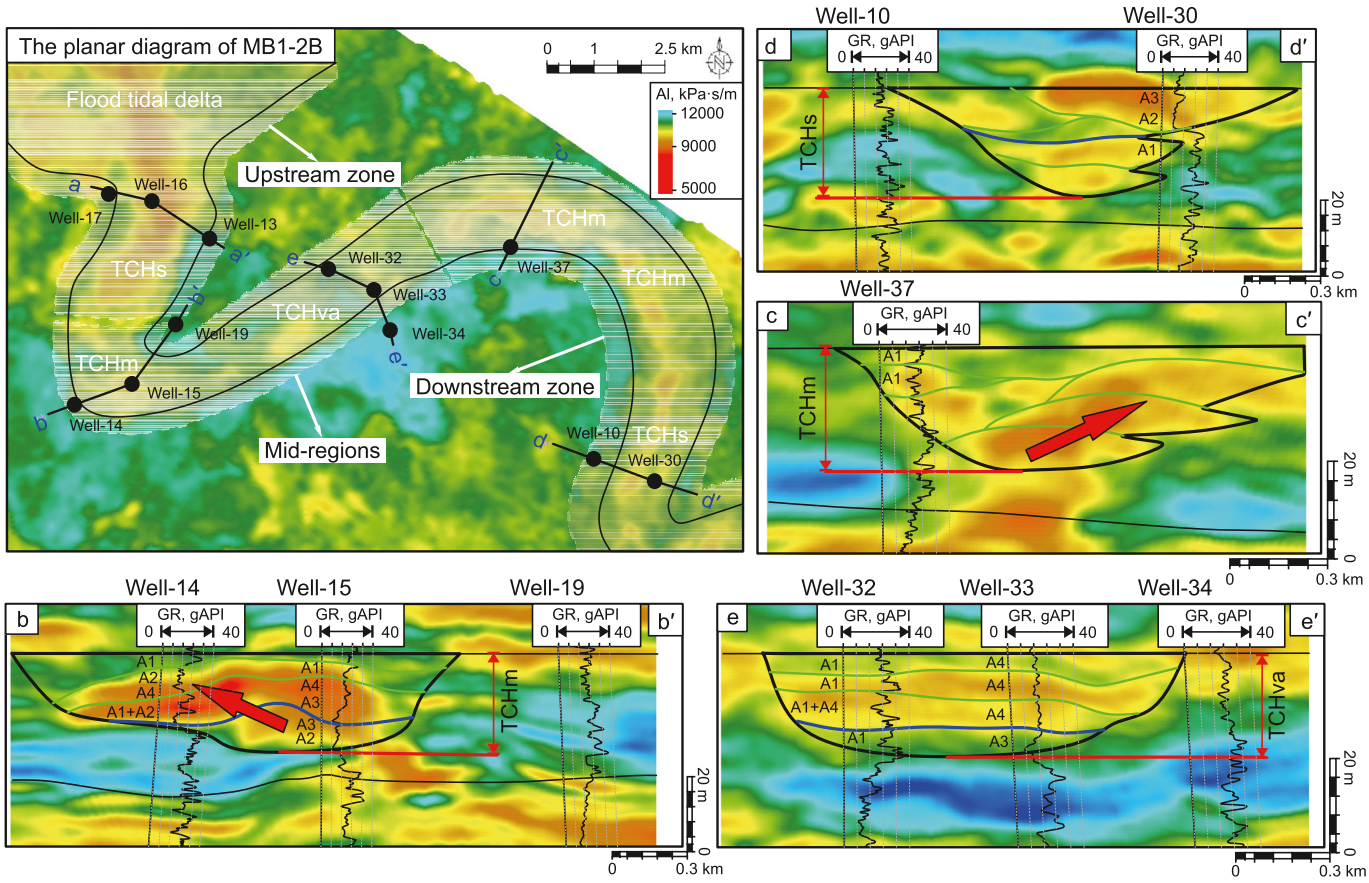

Fig. 8. Profile structure at different positions of tidal channel architecture. The wave impedance inversion map of MB1-2B shows the locations of cored wells and non-cored wells. Wave impedance inversion represents the part reservoir. Sinuous planform geometries are present. The seismic profile of b–b′, c–c′, d–d′, and e–e′ represents five oblique strike sections across a sinuous form (tidal channel). Red arrows indicate the migration direction of the tidal channel.

vertical aggradation feature, the thickness is thin, and the filling lithology is mainly marl (Fig. 8).

5.2. Spatial distribution of tidal channels

Carbonate tidal channels and meandering rivers have similar characteristics, but their differences are also very obvious.

1) For the tidal channel of the carbonate platform, the energy of the ebb current increases due to the existence of the tidal range (Armella et al., 2007), mainly erosion and bedload transport (Ginsberg and Perillo, 1999). In the downstream zone, the tidal channels near the open sea are sinuous, wide, and high-energy (Ferreira et al., 2022) with coarse-grained sediments under the joint result of the lateral erosion and downcutting. The impedance inversion value and GR in the downstream zone are higher than that in the mid-regions (Fig. 8), and the fine-grained sediments within the tidal channel are characterized by the low impedance inversion value and GR (Fig. 8, c–c′, well-37), deposited during periods of tidal channel complex abandonment (Tirsgaard, 1993). Thus, the architecture characteristics are mainly migrating tidal channels (Fig. 8), but the TCHs may occur with the reduction of curvature in the downstream zone (Fig. 8, d–d′).
2) While the width of the tidal channel extending to the lagoon side becomes narrow (Fig. 8), the tidal channels are mainly infilled by fine-grained sediments due to decreasing energy (Hughes, 2012), the architecture characteristics are mainly the vertical-accretion tidal channel in the mid-regions (Fig. 8). The reason is that the energy of flood/ebb current is gradually weakened due to the nearly instantaneous current reversals (Wells et al., 1990) and high geographical position. However, the coarse-grained sediments are still deposited in the bend of the tidal channel (Fig. 8, b–b′), supporting the cognition that the locally shelly/intraclast lags in the channelized zone commonly have mud-covered bottoms (Wu et al., 2021). The seismic attribute slice shows the occurrence of the impedance inversion high-value area with bundles and patch form, representing the coarse-grained sediment (Fig. 8).
3) In the upstream zone, the distribution characteristics of the impedance inversion high-value area with lobate form are observed in the seismic attribute slice (Fig. 8), presumably that is a flood-tidal delta in the inner lagoon (Rivers et al., 2020). Outward from the mid-regions, as relief decreases, the velocities of the flood current are accelerated and easily deposit the coarser-grained bioclasts (Reeder and Rankey, 2009), showing the high-value area of the impedance inversion and GR (Fig. 7). Simultaneously, the channel type grades into a TCHs from a TCHm (Fig. 7), as the restrictions weaken in some outlets is caused by carbonate islands (Reeder and Rankey, 2009), similar to the wide erosive tidal channels explained by Pérez-López et al. (2021). Furthermore, the occurrence of the dolomites and mud drapes at the top of the tidal channel (Figs. 5 and 6), suggests the TCHs develop in a slack water and shallow water stage (Reynaud and James, 2012; Seyedmehdi et al., 2016).

Therefore, the architectural characteristics near the lagoon are mainly swinging tidal channels.

Combined with the fine characterization of the core, logging, and seismic data in the study area, this paper establishes the tidal channel architecture sedimentary model of the carbonate platform (Fig. 9). This model (Fig. 9) mainly shows the internal structure, the plane shape of the tidal channel and its superposition relationship with other architectures. It can be seen from the model diagram that the tidal channel architecture shows a wide and deep swinging tidal channel, asymmetric migrating tidal channel, and narrow and shallow vertical-accretion tidal channel. The grainstone is mainly filled in the filling and swinging tidal channels and the migrating tidal channels, while the marlite is mainly filled in the vertical-accretion tidal channels and the relatively low-energy positions of the swinging and migrating tidal channels. The swinging tidal channel is analogous to a bioclastic Olariu, C., Steel R.J., Olariu M.I., (Fig. 7 in Grélaud et al., 2010), the fill of this channel comprises a complex set of channelized bodies, mainly of grainstone. The migrating tidal channel is akin to a complex of bioclastic channels in the northwestern part of Jabal Madar by offlapping lateral stack of channelized bodies (Fig. 9 in Grélaud et al., 2010), a clear erosive margin is observed on one side. The vertical-accretion tidal channels have been observed in modern tidal channels in the estuaries of Willapa Bay and Oggchee Estuary (Olariu et al., 2015) where sinuosity is low and mud fill.

5.3. Development strategy of tidal channels

The diagenesis of tidal channels was dominated by dissolution, accompanied by typical diagenetic features including suture lines, growth margins, and mud coats (Fig. 6). Large amounts of dolomite were developed at the top of the wackestone and packstone, with an overall porosity of more than 20% (Fig. 4). The dissolution-modified grained carbonate facies were dominated by intergranular and intragranular dissolution pores, showing mesopores (Fig. 6). The dissolution-modified packstone facies were dominated by intergranular solvation pores, with a few solvation pores typical of cast pores, showing the pore sizes dominated by smaller medium-sized pores (Fig. 6). Therefore, the grained carbonates were mainly developed at the sinuous part of the tidal channels and the outlets.

Reservoirs with high permeability were formed at the upstream and downstream parts of the tidal channels, which show the characteristics of high porosity, and high permeability with high degree of dissolution modification (Fig. 4). The inner channels of MB1-2B were connected by layers with low to high permeability. The swinging tidal channels cut shoals were connected by layers with high permeability by the grainstone, including disconnected interlayer. The third-order elements in the swinging-type tidal channel architecture with no recognizable impact on seepage (Fig. 9, a–a'). The migrating tidal channels cut shoals which were connected by high to medium permeability layers on one side with grainstone. The most direct impact of the third-order elements in the migrating-type tidal channel architecture is being felt in the direction of migration, the muddy deposits in the direction of non-migrating impede seepage of the inner channels (Fig. 9, b–b' and d–d'). However, the vertical-accretion tidal channels cut shoals, and all types of tidal channels cut lagoon deposits which were connected by layers with low to medium permeability. Therefore, the well-pattern of wells will give preference to areas near the inner lagoon (i.e., the upstream zone) and open sea (i.e., the downstream zone) for inside the tidal channel (Fig. 9), with the sinuous part and near the side of concave bank for across the tidal channel (Fig. 9). For development strategies, the direction of migration of the third-order elements for the tidal channel should be taken into account when designing the perforated interval of the injection/oil well to improve the injection water contribution or oil contribution.

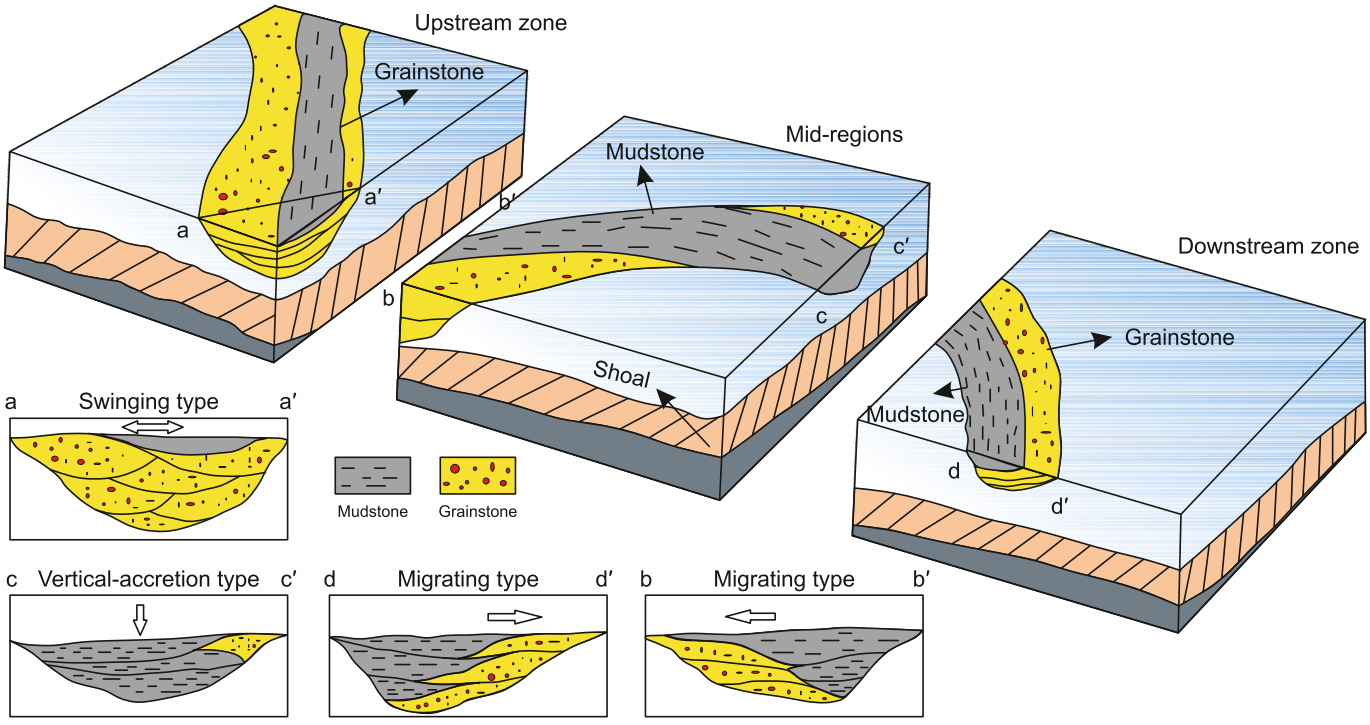

Fig. 9. Sedimentary model of carbonate tidal channel architecture.

6. Conclusions

The MB1-2B sub-layer of the Mishrif Formation in the Late Cretaceous contains tidal channel deposits. In the interval of cored and non-cored, tidal channels of architectural elements, including swinging type, migrating type, and filling type, were identified. Architectural surface and lithofacies assemblages were recognized and correlated based on the logging curve, the relationship between the architectural elements and the filling of lithofacies assemblages was predicted as follows.

(1) For swinging tidal channels, the pattern of vertical filling includes association 2–association 3 + 2 + 4–association 2–association 3 + 1 from bottom to top, and the GR logging response characteristics are bell-shaped to funnel-shaped to blocky-shaped to bell-shaped.
(2) For migrating tidal channels, the style of filling is association 2, and the GR logging response characteristic is blocky-shaped.
(3) For vertical-accretion tidal channel, the style of filling is association 3–association 4–association 1, and the GR logging response characteristics are bell-shaped to blocky-shaped.

Additionally, sedimentary models of the carbonate tidal channel were established to distinguish the swinging type in the upstream zone, the migrating type in the downstream zone, and the vertical-accretion type in the mid-regions for tidal channels in the carbonate platform. The characteristics of spatial distribution are as follows: One side of the gentle slope (or the side of the concave bank) of the architecture of tidal channels is usually filled with relatively coarse-grained grainstone. When the curvature of the tidal channel architecture was high, the interior of the tidal channel was of the migrating type with wide and shallow; when the curvature of the tidal channel architecture was reduced, the interior of the tidal channel was of swinging type with wide and deep; when the curvature of the tidal channel architecture was straight, the interior of the tidal channel was of filling type with symmetrical geometry in cross section.

CRediT authorship contribution statement

Zhan-Feng Qiao: Writing – original draft, Conceptualization. **Guang-Ya Zhu:** Methodology. **Shun-Li Li:** Writing – review & editing. **Guan-Ming Shao:** Investigation. **Wen-Jun Kang:** Methodology, Investigation. **Xiao-Wei Sun:** Methodology. **Qian-Ying Yao:** Methodology. **Yu Zhang:** Methodology.

Declaration of competing interest

No potential conflict of interest was reported by the authors.

Acknowledgment

This study was funded by the PetroChina Science and Technology Major Project (No. 2023ZZ19-1), the PetroChina Science and Technology Development Project (No. 2021DQ0407), the Chinese National Natural Science Fund Project (No. 42272124), and the National Key R&D Program of China (2023YFF0804302). We are thankful to the editorial guidance and anonymous reviewers for insightful reviews that improved the manuscript.

References

Allen, J.R.L., 1983. Studies in fluviatile sedimentation: bars, bar-complexes and sandstone sheets (low-sinuosity braided streams) in the Brownstones (L. Devonian), Welsh Borders. Sediment. Geol. 33, 237–293. https://doi.org/10.1016/0037-0738(83)90076-3.

Al-Qayim, B., 2010. Sequence stratigraphy and reservoir characteristics of the Turonian-Coniacian Khasib formation in central Iraq. J. Pet. Geol. 33, 387–403. https://doi.org/10.1111/j.1747-5457.2010.00486.x.

Alqubalee, A., Muharrag, J., Salisu, A.M., et al., 2022. The negative impact of Ophiomorpha on reservoir quality of channelized deposits in mixed carbonate siliciclastic setting: the case study of the Dam Formation, Saudi Arabia. Mar. Pet. Geol. 140, 105666. https://doi.org/10.1016/j.marpetgeo.2022.105666.

Andreucci, S., Pistis, M., Funedda, A., et al., 2017. Semi-isolated, flat-topped carbonate platform (Oligo-Miocene, Sardinia, Italy): sedimentary architecture and processes. Sediment. Geol. 361, 64–81. https://doi.org/10.1016/j.sedgeo.2017.09.012.

Aqrawi, A.A.M., 1998. Paleozoic stratigraphy and petroleum systems of the western and southwestern deserts of Iraq. GeoArabia 3, 229–248. https://doi.org/10.2113/geoarabia0302229.

Aqrawi, A.A.M., Mahdi, T.A., Sherwani, G.H., et al., 2010. Characterization of the mid-Cretaceous Mishrif reservoir of the southern Mesopotamian basin, Iraq. American Association of Petroleum Geologists Conference and Exhibition 7, 7–10. https://doi.org/10.3997/2214-4609-pdb.248.104.

Armella, C., Cabaleri, N., Leanza, H.A., 2007. Tidally dominated, rimmed-shelf facies of the Picún Leufú formation (Jurassic/Cretaceous boundary) in southwest Gondwana, Neuquén basin, Argentina. Cretaceous Res 28 (6), 961–979. https://doi.org/10.1016/j.cretres.2007.01.001.

Bayet-Goll, A., Geyer, G., Daraei, M., 2018. Tectonic and eustatic controls on the spatial distribution and stratigraphic architecture of late early Cambrian successions at the northern Gondwana margin: the siliciclastic-carbonate successions of the Lalun Formation in central Iran. Mar. Pet. Geol. 98, 199–228. https://doi.org/10.1016/j.marpetgeo.2018.08.002.

Bluck, B.J., 1979. Structure of coarse-grained braided stream alluvium. Earth Environ. Sci. Trans. R. Soc. Edinburgh 70, 181–221. https://doi.org/10.1017/S0080456800012795.

Bosence, D., Gibbons, K.A., Heron, D., et al., 2015. Microbial carbonates in space and time: implications for global exploration and production. Geol. Soc. Spec. Publ. 418, 221–242. https://doi.org/10.1144/SP418.

Bridge, J.S., 1993. The interaction between channel geometry, water flow, sediment transport and deposition in braided rivers. Geol. Soc. Spec. Publ. 75, 13–71. https://doi.org/10.1144/GSL.SP.1993.075.01.02.

Bridge, J.S., 2003. Rivers and Floodplains: Forms, Processes, and Sedimentary Record. Oxford, Blackwell, p. 416.

Bridge, J.S., Lunt, I.A., 2006. Depositional models of braided rivers. In: Braided Rivers: Process, Deposits, Ecology and Management, pp. 11–50. https://doi.org/10.1002/9781444304374.ch2.

Cant, D.J., Walker, R.G., 1978. Fluvial processes and facies sequences in the sandy braided South Saskatchewan River, Canada. Sedimentology 25, 625–648. https://doi.org/10.1111/j.1365-3091.1978.tb00323.x.

Chang, S.Y., Sheng, A.J., Qiao, Z.F., et al., 2018. Key technology and application of configuration characterization of reef and shoal reservoir in rimmed platform – taking Lianglitage Formation in Tazhong as an example. Proceedings of the 15th National Academic Conference on Palaeogeography and Sedimentology, pp. 297–298.

Chen, H.Q., Shi, C.F., Cao, C., 2015. Advances in the study of fine reservoir description. Geol. Rev. 61, 1135–1146 (in Chinese).

Chen, Q., Kavanaugh, J., Gingras, M.K., et al., 2022. Recognizing genetically related depositional packages using 3D photogrammetric outcrop models in a fluvially dominated, tidally influenced meander-belt succession. Sediment. Geol. 442, 106288. https://doi.org/10.1016/j.sedgeo.2022.106288.

Davis, R.A., Dalrymple, R.W. (Eds.), 2012. Principles of Tidal Sedimentology. Springer, New York, p. 621.

Donnici, S., Madricardo, F., Serandrei-Barbero, R., 2017. Sedimentation rate and lateral migration of tidal channels in the Lagoon of Venice (Northern Italy). Estuar Coast Shelf S. 198, 354–366. https://doi.org/10.1016/j.ecss.2017.02.016.

Dunham, R.J., 1962. Classification of Carbonate rocks according to depositional texture. AAPG Memoir 1, 108–121.

Dunnington, H.V., 2005. Generation, migration, accumulation, and dissipation of oil in Northern Iraq. GeoArabia 10, 39–84. https://doi.org/10.2113/geoarabia100239.

Embry, A.F., Klovan, J.E., 1971. A late devonian reef tract on northeastern banks island, northwest territories. B Can Petrol Geol. 19, 730–781. https://doi.org/10.35767/gscpgbull.19.4.730.

Ferreira, A.L., Vital, H., Stattegger, K., et al., 2022. Seismic architecture of the tidal channel system of Galinhos, equatorial Atlantic, Brazil. Mar. Geol. 443, 106685. https://doi.org/10.1016/j.margeo.2021.106685.

Flügel, E., 2004. Facies of Carbonate Rocks. Analysis, Interpretation and Application. Springer, p. 976.

Ginsberg, S.S., Perillo, G.M., 1999. Deep-scour holes at tidal channel junctions, Bahia Blanca Estuary, Argentina. Mar. Geol. 160 (1–2), 171–182. https://doi.org/10.1016/S0025-3227(99)00019-5.

Grélaud, C., Razin, P., Homewood, P.W., et al., 2006. Development of incisions on a periodically emergent carbonate platform (natih formation, late cretaceous, Oman). J. Sediment. Res. 76, 647–669. https://doi.org/10.2110/jsr.2006.058.

Grélaud, C., Razin, P., Homewood, P., 2010. Channelized systems in an inner carbonate platform setting: differentiation between incisions and tidal channels (Natih Formation, Late Cretaceous, Oman). Geol. Soc. Spec. Publ. 329, 163–186. https://doi.org/10.1144/SP329.8.

Harris, P.T., Heap, A., Passlow, V., et al., 2005. Tidally incised valleys on tropical carbonate shelves: an example from the northern Great Barrier Reef, Australia. Mar. Geol. 220 (1–4), 181–204. https://doi.org/10.1016/j.margeo.2005.06.019.
Hashemi, S., Javaherian, A., Ataee-pour, M., et al., 2014. Channel characterization using multiple-point geostatistics, neural network, and modern analogy: a case study from a carbonate reservoir, southwest Iran. J. Appl. Geophys. 111, 47–58. https://doi.org/10.1016/j.jappgeo.2014.09.015.
Hein, F.J., Leckie, D., Larter, S., et al. (Eds.), 2013. Heavy Oil and Oil-Sand Petroleum Systems in Alberta and beyond. AAPG Studies in Geology 64, p. 131. https://doi.org/10.1306/St641337.
Hubbard, S.M., Smith, D.G., Nielsen, H.A., et al., 2011. Seismic geomorphology and sedimentology of a tidally influenced river deposit, Lower Cretaceous Athabasca oil sands, Alberta, Canada. AAPG Bull. 95, 1123–1145. https://doi.org/10.1306/12131010111.
Hughes, Z.J., 2012. Tidal channels on tidal flats and marshes. In: Davis Jr., R., Dalrymple, R. (Eds.), Principles of Tidal Sedimentology. Springer, Dordrecht. https://doi.org/10.1007/978-94-007-0123-6_11.
Jin, D.W., 2009. Application of reservoir composition unit analysis method in fine stratigraphic correlation of carbonate beach bar reservoir. Petroleum Geology and Engineering 23, 56–58 (in Chinese).
Kargarpour, M.A., 2020. Carbonate reservoir characterization: an integrated approach. J. Pet. Explor. Prod. Technol. 10, 2655–2667. https://doi.org/10.1007/s13202-020-00946-w.
Kerans, C., 1988. Karst-controlled reservoir heterogeneity in Ellenburger Group carbonates of west Texas. AAPG Bull. 72, 1160–1183. https://doi.org/10.1306/703C996F-1707-11D7-8645000102C1865D.
Léonide, P., Fournier, F., Reijmer, J.J.G., et al., 2014. Diagenetic patterns and pore space distribution along a platform to outer-shelf transect (Urgonian limestone, Barremian–Aptian, SE France). Sediment. Geol. 306, 1–23. https://doi.org/10.1016/j.sedgeo.2014.03.001.
Li, F., Zhang, N., Xia, W.C., 2010. Carbonate facies analysis on chihsia formation (middle permian) at Xiakou area, western Hubei Province. Geol. Sci. Technol. Inf. 29, 23–28. https://doi.org/10.3969/j.issn.1000-7849.2010.01.004 (in Chinese).
Li, S.L., Yu, X.H., Chen, B.T., et al., 2015. Quantitative characterization of architecture elements and their response to base-level change in a sandy braided fluvial system at a mountain front. J. Sediment. Res. 85, 1258–1274. https://doi.org/10.2110/jsr.2015.82.
Lunt, I.A., Bridge, J.S., 2004. Evolution and deposits of a gravelly braid bar, Sagavanirktok River, Alaska. Sedimentology 51, 415–432. https://doi.org/10.1111/j.1365-3091.2004.00628.x.
Mahdi, T.A., Aqrawi, A.A., Horbury, A.D., et al., 2013. Sedimentological characterization of the mid-Cretaceous Mishrif reservoir in southern Mesopotamian Basin, Iraq. GeoArabia 18 (1), 139–174. https://doi.org/10.2113/geoarabia1801139.
Mahdi, T.A., Aqrawi, A., 2014. Sequence stratigraphic analysis of the mid-cretaceous mishrif formation, southern Mesopotamian Basin, Iraq. J. Pet. Geol. 37, 287–312. https://doi.org/10.1111/jpg.12584.
Miall, A.D., 1977. A review of the braided-river depositional environment. Earth Sci. Rev. 13, 1–62. https://doi.org/10.1016/0012-8252(77)90055-1.
Miall, A.D., 1985. Architectural-element analysis: a new method of facies analysis applied to fluvial deposits. Earth Sci. Rev. 22, 261–308. https://doi.org/10.1016/0012-8252(85)90001-7.
Miall, A.D., 1988. Reservoir heterogeneities in fluvial sandstones: lessons from outcrop studies. AAPG Bull. 72, 682–697. https://doi.org/10.1306/703C8F01-1707-11D7-8645000102C1865D.
Miall, A.D., 1992. Alluvial deposits. In: Walker, R.G., James, N.P. (Eds.), Facies Models: Response to Sea Level Change. Geological Association of Canada, pp. 157–178.
Miall, A.D., 1993. Hierarchies of architectural units in terrigenous clastic rocks: a framework for the analysis of fluvial deposits. In: 29th International Geological Congress Meeting, Transactions, p. 293.
Miall, A.D., 1996. The geology of fluvial deposits: sedimentary facies. Basin Analysis and Petroleum Geology. Springer-Verlag, Heidelberg, p. 582.
Miall, A.D., 2014. Fluvial Depositional Systems. Springer-Verlag, Berlin, p. 316.
Miall, A.D., 2022. Stratigraphy: a modern synthesis. Springer Nature, 157–165.
Moore, C.H., 2001. Carbonate reservoirs: porosity evolution and diagenesis in a sequence tratigraphic framework. Elsevier, New York, p. 444.
Noureldin, A.M., Mabrouk, W.M., Metwally, A., 2023. Delineating tidal channel feature using integrated post-stack seismic inversion and spectral decomposition applications of the Upper Cretaceous reservoir Abu Roash C: a case study from Abu-Sennan oil field, Western Desert, Egypt. J. Afr. Earth Sci. 205, 104974. https://doi.org/10.1016/j.jafrearsci.2023.104974.
Olariu, C., Steel, R.J., Olariu, M.I., et al., 2015. Facies and architecture of unusual fluvial–tidal channels with inclined heterolithic strata: campanian Neslen Formation, Utah, USA. Dev. Sedimentol. 68, 353–394. https://doi.org/10.1016/B978-0-444-63529-7.00011-0.
Owen, R., Nasr, S.N., 1958. Habitat of oil. In: Weeks, L.G. (Ed.), Stratigraphy of the Kuwait–Basrah Area. AAPG symposium, pp. 1252–1278. https://doi.org/10.1306/SV18350C50.
Pérez-López, A., Benedicto, C., Ortí, F., 2021. Middle triassic carbonates of eastern iberia (western tethyan realm): a shallow platform model. Sediment. Geol. 420, 105904. https://doi.org/10.1016/j.sedgeo.2021.105904.
Pratt, B.R., Rule, R.G., 2021. A Mesoproterozoic carbonate platform (lower Belt Supergroup of western North America): sediments, facies, tides, tsunamis and earthquakes in a tectonically active intracratonic basin. Earth Sci. Rev. 217, 103626. https://doi.org/10.1016/j.earscirev.2021.103626.
Purkis, S., 2019. Emergent behavior and emerging methods in carbonate depositional environments//Abstracts of 34th IAS International Meeting of Sedimentology, vol. 169. IAS, Rome.
Qiao, Z.F., Janson, X., Shen, A.J., et al., 2016. Lithofacies, architecture, and reservoir heterogeneity of tidal-dominated platform marginal oolitic shoal: an analogue of oolitic reservoirs of Lower Triassic Feixianguan Formation, Sichuan Basin, SW China. Mar. Pet. Geol. 76, 290–309. https://doi.org/10.1016/j.marpetgeo.2016.05.030.
Qiao, Z.F., Shen, A.J., Zheng, J.F., et al., 2017. Digitized outcrop geomodeling of ramp shoals and its reservoirs: as an example of lower triassic feixianguan Formation of eastern sichuan basin. Acta Geol Sin-Engl. 91, 1395–1412. https://doi.org/10.1111/1755-6724.13369.
Rahmani, R.A., De Boer, P.L., Van Gelder, A., et al., 1988. Tide-Influenced sedimentary environments and facies. In: de Boer, P.L., van Gelder, A., Nio, S.D. (Eds.), Estuarine tidal channel and nearshore sedimentation of a Late Cretaceous epicontinental sea, Drumheller. D. Reidel Publishing Company, Dordrecht, Alberta, Canada, pp. 433–471.
Rankey, E.C., 2003. Carbonate-filled channel complexes on carbonate ramps: an example from the peerless park member [keokuk limestone, visean, lower carboniferous (mississippian)], St. Louis, MO, USA. Sediment. Geol. 155 (1–2), 45–61. https://doi.org/10.1016/S0037-0738(02)00158-6.
Read, J.F., 1982. Carbonate platforms of passive (extensional) continental margins: types, characteristics and evolution. Tectonophysics 81, 195–212. https://doi.org/10.1016/0040-1951(82)90129-9.
Rebata, L., Gingras, M., Räsänen, M., et al., 2006. Tidal-channel deposits on a delta plain from the upper miocene nauta formation, Marañon foreland sub-basin, Peru. Sedimentology 53, 971–1013. https://doi.org/10.1111/j.1365-3091.2006.00795.x.
Reeder, S.L., Rankey, E.C., 2009. Controls on morphology and sedimentology of carbonate tidal deltas, Abacos, Bahamas. Mar. Geol. 267 (3–4), 141–155. https://doi.org/10.1016/j.margeo.2009.09.010.
Reynaud, J.Y., James, N.P., 2012. The Miocene Sommières basin, SE France: bioclastic carbonates in a tide-dominated depositional system. Sediment. Geol. 282, 360–373. https://doi.org/10.1016/j.sedgeo.2012.10.006.
Rivers, J.M., Dalrymple, R.W., Yousif, R., et al., 2020. Mixed siliciclastic-carbonate-evaporite sedimentation in an arid eolian landscape: the Khor Al Adaid tide-dominated coastal embayment, Qatar. Sediment. Geol. 408, 105730. https://doi.org/10.1016/j.sedgeo.2020.105730.
Roehl, P.O., Choquette, P.W., 1985. Perspectives on world-class carbonate petroleum reservoirs. AAPG Memoir 69, 148. https://doi.org/10.1306/AD461C64-16F7-11D7-8645000102C1865D.
Sabouhi, M., Moussavi-Harami, R., Kadkhodaie, A., et al., 2023. Stratigraphic influences on reservoir heterogeneities of the Mid-Cretaceous carbonates in southwest Iran: insight from an integrated stratigraphic, diagenetic and seismic attribute study. J. Asian Earth Sci. 243, 105514. https://doi.org/10.1016/j.jseaes.2022.105514.
Sadooni, F.N., 2005. The nature and origin of Upper Cretaceous basin-margin rudist buildups of the Mesopotamian Basin, southern Iraq, with consideration of possible hydrocarbon stratigraphic entrapment. Cretaceous Res 26, 213–224. https://doi.org/10.1016/j.cretres.2004.11.016.
Salehi, M.A., Bahrami, A., Moharrami, S., et al., 2020. Palaeoenvironmental and sequence-stratigraphic analysis of the middle–late devonian carbonates (bahram formation) of Anarak, western Central Iran. J. Afr. Earth Sci. 171, 103938. https://doi.org/10.1016/j.jafrearsci.2020.103938.
Seyedmehdi, Z., George, A.D., Tucker, M.E., 2016. Sequence development of a latest Devonian–Tournaisian distally-steepened mixed carbonate–siliciclastic ramp, Canning Basin, Australia. Sediment. Geol. 333, 164–183. https://doi.org/10.1016/j.sedgeo.2015.12.012.
Shen, A.J., Chen, Y.N., Meng, S.X., et al., 2019. The research progress of marine carbonate reservoirs in China and its significance for oil and gas exploration. Marine Origin Petroleum Geology 24, 1–14. https://doi.org/10.3969/j.issn.1672-9854.2019.04.001 (in Chinese).
Sun, W.J., Qiao, Z.F., Shao, et al., 2020. Sedimentation and reservoir architecture of MB1-2 submember of middle cretaceous mishrif Formation in halfaya oilfield. Iraq. Pet. Explor. Dev. 47, 713–722. https://doi.org/10.1016/S1876-3804(20)60091-X.
Tirsgaard, H., 1993. The architecture of Precambrian high energy tidal channel deposits: an example from the Lyell Land Group (Eleonore Bay Supergroup), northeast Greenland. Sediment. Geol. 88 (1–2), 137–152. https://doi.org/10.1016/0037-0738(93)90154-W.
Walker, R.G., Cant, D.J., 1984. Sandy fluvial systems. In: Walker, R.G. (Ed.), Facies Models, second ed., pp. 71–89 Toronto, Geoscience Canada.
Wang, Y.X., Zhou, W., Guo, R., 2016. Rock types and characteristics of the Middle-Upper Cretaceous carbonate reservoirs in Halfaya oilfield. Iraq. Oil & Gas Geology 37 (5), 764–772. https://doi.org/10.11743/ogg20160516 (in Chinese).
Wells, J.T., Adams, C.E., Park, et al., 1990. Morphology, sedimentology and tidal channel processes on a high-tide-range mudflat, west coast of South Korea. Mar. Geol. 95 (2), 111–130. https://doi.org/10.1016/0025-3227(90)90044-K.
Williams, P.F., Rust, B.R., 1969. The sedimentology of a braided river. J. Sediment. Petrol. 39, 649–679. https://doi.org/10.1306/74D71CF3-2B21-11D7-8648000102C1865D.
Wilson, J.L., 1975. Carbonate Facies in Geologic History. Springer, pp. 348–374.
Wu, M., Harris, P.M., Eberli, G., et al., 2021. Sea-level, storms, and sedimentation–controls on the architecture of the andros tidal flats (great

bahama bank). Sediment. Geol. 420, 105932. https://doi.org/10.1016/j.sedgeo.2021.105932.
Xu, J.L., Hong, T.Q., Jia, Z.H., et al., 2012. The characteristics of storm deposits in the lower Huanglong Formatiom of Majiaoba area, northwestern Sichuan Provine. Chinese Journal of Geology 47, 422–439 (in Chinese).
Yang, C.Y., Wu, C.D., 1998. A study on sedimentary diagenetic facies of carbonate rocks of Ordovician Majiagou formation in Ordos Basin. Earth Sci. Front. 4, 79–85 (in Chinese).
Yu, Y.C., Sun, L.D., Song, X.M., et al., 2018. Sedimentary diagenesis of rudist shoal and its control on reservoirs: a case study of Cretaceous Mishrif Formation, H Oilfield, Iraq. Petrol. Explor. Dev. 45, 1007–1019. https://doi.org/10.11698/PED.2018.06.08 (in Chinese).
Zhao, W.Z., Shen, A.J., Hu, S.Y., et al., 2012. Geological conditions and distributional features of large-scale carbonate reservoirs onshore China. Petrol. Explor. Dev. 39 (1), 1–14. https://doi.org/10.1016/S1876-3804(12)60010-X (in Chinese).
Zhu, X.M., Dong, Y.L., Liu, C.L., et al., 2021. Major challenges and development in Chinese sedimentological research on petroliferous basins. Earth Sci. Front. 28, 1–11. https://doi.org/10.13745/j.esf.sf.2020.5.1 (in Chinese).